Nucleotide Binding Modes in a Motor Protein Revealed by 31 P- and 1 H-Detected MAS Solid-State NMR Spectroscopy

Thomas Wiegand, Maarten Schledorn, Alexander A Malär, Riccardo Cadalbert, Alexander Däpp, Laurent Terradot, Beat H Meier, Anja Böckmann

A EUROPEAN JOURNAL OF CHEMICAL BIOLOGY

CHEMBIOCHEM

SYNTHETIC BIOLOGY & BIO-NANOTECHNOLOGY

Accepted Article

Title: Nucleotide binding modes in a motor protein revealed by 31P- and 1H-detected MAS solid-state NMR

Authors: Thomas Wiegand, Maarten Schledorn, Alexander A. Malär, Riccardo Cadalbert, Alexander Däpp, Laurent Terradot, Beat H. Meier, and Anja Böckmann

To be cited as: *ChemBioChem* 10.1002/cbic.201900439

Link to VoR: http://dx.doi.org/10.1002/cbic.201900439

A Journal of

ChemPubSoc Europe

WILEY-VCH

www.chembiochem.org

10.1002/cbic.201900439

Nucleotide binding modes in a motor protein revealed by ^{31}P- and ^{1}H-detected MAS solid-state NMR

Thomas Wiegand[a,*], Maarten Schledorn[a], Alexander A. Malär[a], Riccardo Cadalbert[a], Alexander Däpp[a], Laurent Terradot[b], Beat H. Meier[a] and Anja Böckmann[b,*]

[a] *Physical Chemistry, ETH Zurich, 8093 Zurich, Switzerland*

[b] *Molecular Microbiology and Structural Biochemistry, Labex Ecofect, UMR 5086 CNRS/Université de Lyon 69367 Lyon, France*

[*]Corresponding authors: thomas.wiegand@phys.chem.ethz.ch, a.bockmann@ibcp.fr

Abstract

Protein-nucleic acid interactions play important roles not only in energy-providing reactions such as ATP hydrolysis, but also in reading, extending, packaging or repairing genomes. While they can often be analyzed in detail with X-ray crystallography, complementary methods are needed to visualize them in complexes which are not crystalline. We here show how solid-state NMR can detect and classify protein-nucleic interactions via site-specific ^{1}H- and ^{31}P-detected spectroscopies. The sensitivity of ^{1}H chemical-shift values on non-covalent interactions involved in these molecular recognition processes is exploited allowing us to probe directly the chemical bonding state, an information which is not directly accessible from an X-ray structure. We show that these methods can characterize interactions in easy-to-prepare sediments of the 708 kDa dodecameric DnaB helicase in complex with ADP:AlF_4^-:DNA, and this despite the very challenging size of the complex.

Keywords

DnaB helicase, Fast MAS, Hydrogen bonds, Nucleotide-binding, solid-state NMR

Graphical Abstract

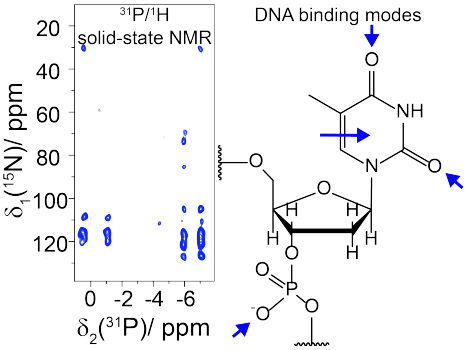

Protein-nucleotide contacts in a non-crystalline bacterial DnaB helicase sedimented in the NMR rotor were probed by ^{31}P- and ^{1}H-detected solid-state NMR spectroscopy. The sensitivity of ^{1}H chemical shifts to hydrogen bonding was explored and used to identify residues involved in nucleotide coordination. In combination with phosphorus-proton proximities identified by heteronuclear correlation experiments, a detailed binding model for DNA and ADP:AlF_4^- to DnaB was derived.

Nucleotide-protein interactions play a central role in two major biological functions: in energy-providing reactions, where ATP is hydrolyzed to yield energy to motor domains driving reactions[1-2]; and in interactions with RNA or DNA, central in a large variety of biomolecular functions. Binding of nucleotides, such as ATP and DNA, occurs via non-covalent interactions including hydrogen bonds, electrostatic (salt bridges) and van-der-Waals interactions[3-4] (the latter also comprising interactions between aromatic rings[5]). These interactions have been typically studied in the past by high-resolution X-ray crystallography[4, 6-7]. Still, many of the above-described scenarios involve protein complexes which are difficult to crystallize, and when they do so, might reflect at insufficient resolution to clearly identify interactions. Alternative methods are therefore needed and can be provided through solid-state NMR, which can access also large biomolecular complexes, and importantly in sample formats where the assemblies are simply sedimented into the NMR rotor[8]. And indeed, solid-state NMR has been used to identify residues at protein-RNA interfaces in smaller proteins[9-12].

Two approaches are particularly promising to probe nucleotide interactions: phosphorus- (^{31}P) and proton- (^{1}H) detected spectroscopy. Distances between ^{31}P spins of DNA and ^{15}N spins of a protein have been measured using TEDOR experiments[9]. Intermolecular information can also be obtained from ^{31}P-detected, heteronuclear correlation experiments probing the spatial proximity of nucleotide ^{31}P and protein ^{15}N or ^{13}C nuclei[9, 13]. Proton-detected solid-state NMR spectroscopy at fast MAS frequencies has emerged in the last years and needs today only a few hundred micrograms of fully protonated protein sample[14-23]. Proton chemical-shift values are highly sensitive to hydrogen bonding[24-27] as shown in theoretical[26-27], but also in experimental studies[24-25, 28]. Empirical correlations between the ^{1}H chemical-shift values of amide as well as aliphatic protons[29] and the strength of the hydrogen bond (characterized by the hydrogen bond distance) have been established for biological systems[27, 29-32]. Still, one has to keep in mind that proton chemical shifts can further be influenced by anisotropic neighbor effects, ring current effects[33-35] and the secondary structure[36]. This underlines the importance of combination with evidence from ^{31}P correlations delivering direct geometric information.

We herein use the dodecameric bacterial DnaB helicase from *Helicobacter pylori* with a molecular weight of 12*59 kDa[37] as a model to establish approaches to identify protein-nucleic-acid interactions in large proteins by solid-state NMR. DnaB helicases are motor proteins which coordinate both ATP and DNA[1]: ATP and a Mg^{2+} cofactor are bound by the Walker A and B motifs as well as the arginine finger (R-finger) connecting two adjacent

subunits of the oligomeric assembly[38], whereas DNA binds in the central space of the hexameric proteins to so-called DNA binding loops. It has been revealed from crystal structures[4, 6, 39] that major coordination partners are Lys and Arg side-chains. On the DNA side, important recognition motifs are hydrogen bonds or electrostatic interactions (salt bridges)[40-43] involving the DNA phosphate groups as hydrogen bond acceptors, but also the ribose or the base moieties[4]. We previously established that in DnaB from *Helicobacter pylori*, the ATP hydrolysis transition state, mimicked by ADP:AlF_4^-, preorganizes the helicase for binding single-stranded DNA to the C-terminal domain (CTD)[44]. Upon DNA binding, a large fraction of the protein covering the DNA binding loops stiffens, among them 357R and 373K, potentially involved in DNA binding[44]. We formerly sequentially assigned 70 % of the N-terminal domain (NTD)[45] and approximately 60 % of the CTD (311 residues) of DnaB (^{15}N, ^{13}Cα and ^{13}Cβ, BMRB accession number 27879) using ^{13}C detection. Also, we previously observed that the NTD is not observed in the DnaB:ADP:AlF_4^-:DNA sample, likely due to dynamics, which reduces the number of observed spins to the CTD[44].

We here describe the ^{1}H resonance assignment of the protein (~45 % of the CTD, see BMRB accession number 27879 and Table S1), and record ^{31}P-^{15}N/^{13}C heteronuclear correlation spectra. We show how these data can be used to reveal nucleotide-protein interactions, and to determine binding modes, in particular whether DNA coordinates to DnaB via the phosphate groups or base edges. We identify key residues involved in ATP and DNA binding located in the Walker A motif and the DNA binding loops, and compare them to data described for DnaB from *Bacillus stearothermophilus* (*Bst*DnaB)[7], where a crystal structure is available of the GDP:AlF_4^-:DNA-bound state.

H^N and H^A detected two-dimensional hNH and hCH spectra of DnaB:ADP:AlF_4^-:DNA recorded at an MAS frequency of 110 kHz show a significant number of resolved signals, and are shown in Figure 1a and 2b. For resonance assignments, 3D hCANH, hNCAH, hCAcoNH and hNcoCAH experiments were recorded. The assignment strategy is illustrated in Figure 1b. It allows to walk along the protein backbone and delivers the H^N, H^A, Cα and N chemical shifts. Each correlation between a pair of nuclei appears in two independent experiments, as already proven central in ^{13}C-detected experiments[46]. Figure 1c shows 2D planes of the 3D spectra illustrating the assignment strategy at the example of residues 448G to 450T (for a second example see Figure S1). Around 45 % of the CTD H^N and H^A resonances (142 and 139 resonances, respectively) could be assigned, most of them in a sequential manner (100 and 118 correlations, respectively, in the inter-residual hCAcoNH and hNcoCAH spectra were assigned for which the sequential walk sketched in Figure 1b was performed

successfully), the others by transferring the ^{15}N and ^{13}CA assignments obtained by ^{13}C-detected experiments to the ^{1}H-detected ones. The largest fraction of the NTD remains invisible in ^{1}H-detected spectra as well as in ^{13}C detection[44].

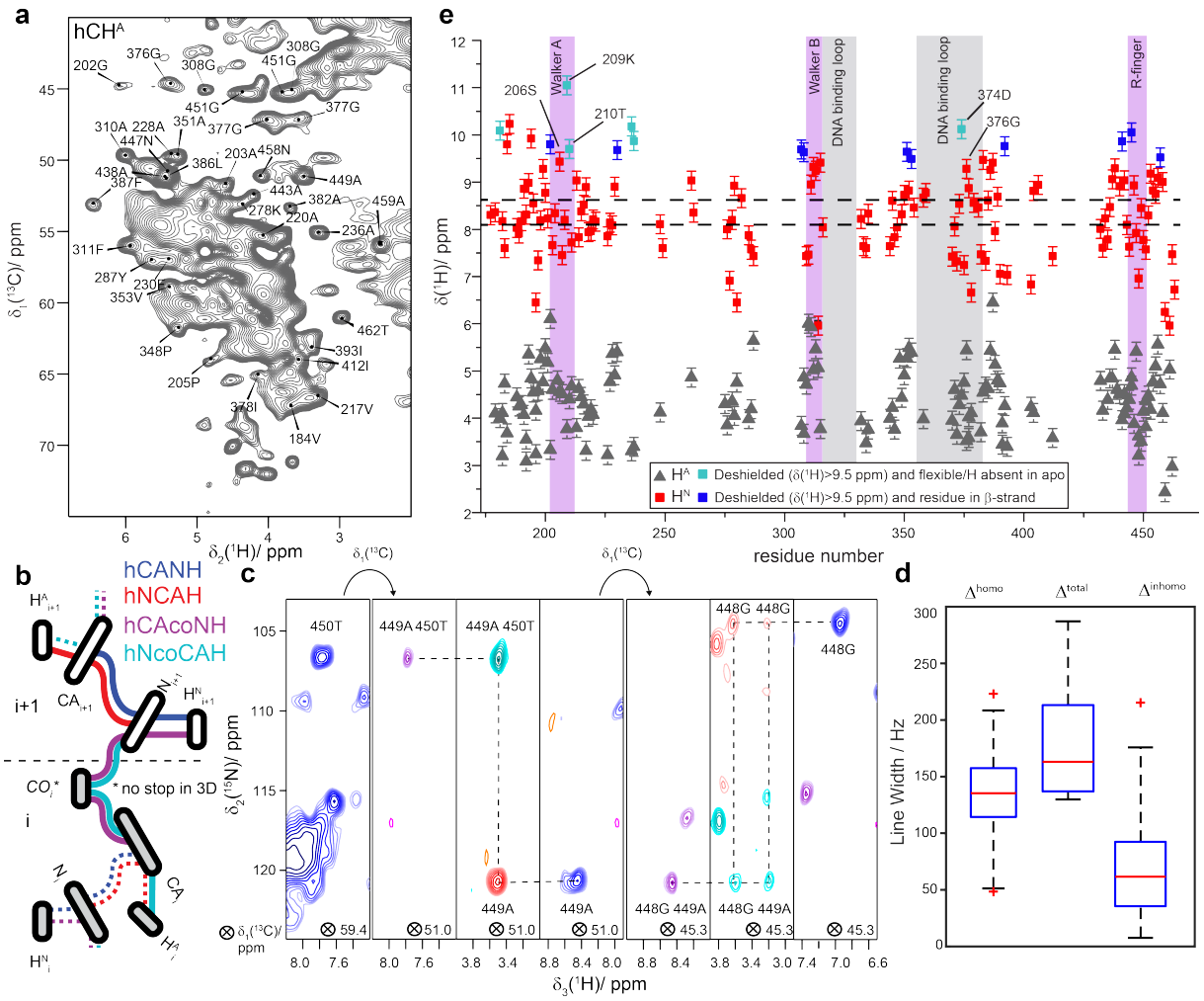

Figure 1: **Sequential assignments of the proton resonances. a** 2D hCH spectrum with assignments of isolated resonances. **b** Assignment strategy using both, H^N and H^A protons. The dashed lines highlight connectivities at the same ^{13}C resonance frequency. **c** Representative 2D planes of 3D spectra used for sequential resonance assignment (backbone "walk"). **d** Boxplots for the ^{1}H homogeneous, the total and the inhomogeneous line width, respectively (see also SI). **e** Site-specific H^N and H^A chemical-shift values. The dashed horizontal lines represent the average H^N shifts in α-helices (8.1 ppm) and β-strands (8.6 ppm)[47]. The error bars are estimated to 0.1 ppm.

The ease of ^{1}H assignments strongly depends on the observed ^{1}H line-widths (Δ^{tot}) which is the sum of homogeneous (Δ^{homo}) and inhomogeneous (Δ^{inhomo}) contributions[48] (see Supplementary Materials Section and Figures S2-S4). Figure 1d shows the contributions to the ^{1}H-line-widths determined for isolated peaks in the 2D hNH spectrum (see Figure S3). The average total line-width of Δ^{tot}=200±50 Hz contains on average a homogeneous broadening of Δ^{homo}=140±40 Hz, which is comparable to other protonated systems[48-49]. The

inhomogeneous contribution is on average Δ^{inhomo}=90±60 Hz. The assigned H^N and H^A chemical shifts are plotted in Figure 1e, and are shown on a structural model of the CTD of the DnaB helicase[37] in Figure 3, color-coded with the corresponding ^{1}H chemical-shift values. Note that the H^N chemical shifts show a quite large spectral dispersion (e.g. ~5 ppm) which is attributed to the high sensitivity of proton shifts to non-covalent interactions: shielded resonances associated with ring-current effects (e.g. 314Y in the Walker B motif and 459A, 461F and 463R possibly located in a loop above the ADP base plane) and deshielded resonances due to hydrogen bond formation (many of them located in β-strands, see Figures 1e and 3 and Figure S5). Assignments of outlier resonances are shown in Figure 1a and Figure 2a. For both ^{1}H species residues in β-strands were nearly completely assigned, while many residues in α-helices remain unassigned. This is a consequence of the larger chemical-shift dispersion of β-strand residues, but also of the usually broader homogeneous ^{1}H lines of residues in α-helices due to a denser proton network[15].

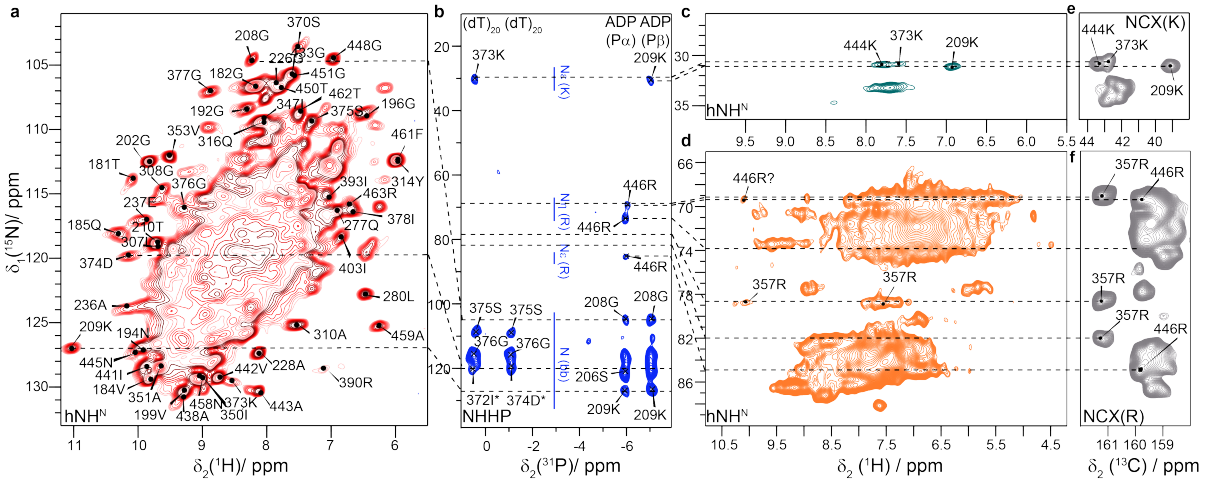

Figure 2: **Solid-state NMR spectra to probe protein-nucleotide interactions. a** 2D hNH spectrum with assignment of isolated resonances. **b** NHHP spectrum with assigned resonances. The Figure is taken in parts from reference [44]. **c** Lysine sidechain 2D hNH spectrum with assignments. **d** Arginine sidechain 2D hNH spectrum with assignments. **e** Lysine sidechain 2D NC spectrum with assignments, from reference [44]. **f** Arginine sidechain 2D NC spectrum with assignments, from reference [44]. Dashed lines are guidance for the eye for the correlations discussed in the text.

To further analyze nucleotide binding, spectra were recorded on two additional protein samples: the apo protein (no nucleotides bound) and DnaB:AMP-PCP:DNA using a pre-hydrolytic ATP-mimic[44].

10.1002/cbic.201900439

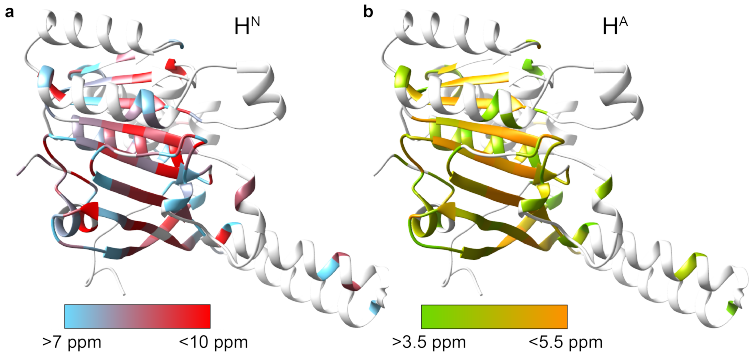

Figure 3: *Proton assignment plotted on a structural model.* **a** Assigned H^N resonances plotted on a DnaB model based on the *Aa*DnaB:ADP complex (PDB 4NMN) using the color code shown in the legend. **b** Assigned H^A resonances plotted on the same model using the color code shown in the legend.

In order to complement the information from the chemical shift, we established direct polarization transfer between spins in spatial proximity (< 8-9 Å), and performed a ^{31}P-detected 2D NHHP (Figure 2b) correlation experiment (for a CHHP spectrum see Figure S6). Compared to the previously described ^{31}P,^{15}N TEDOR experiment used for identifying protein-RNA contacts in a smaller test system[9], the polarization in NHHP experiments is mediated between close-by ^{15}N and ^{31}P nuclei via H-H spin diffusion, which allows to extract medium-to-long-range structural restraints[50] and is thus an alternative to TEDOR experiments. Sensitivity in such experiments is becoming an issue if the ^{31}P spin concentration is small as in the investigated system. The spectra reveal correlations between phosphate groups and backbone amides, as well as arginine and lysine sidechain nitrogen atoms. The spectrum clearly distinguishes different ^{31}P shifts for ADP and DNA[44]. As a matter of fact, assignments in the 2D spectrum remain ambiguous for such a large protein, but could be resolved considering the primary amino-acid sequence and the motifs to which nucleotides were predicted to bind [37] (i.e. residues 203A-210T, 445N-451G and residues 371D-382A[51], respectively), and taking also further NMR spectroscopic information into account (e.g. CSPs and dynamic changes upon nucleotide binding, see reference [44]).

The residue 209K is located in the Walker A motif. A clear 209K N^{ζ}-ADP P^{β} cross signal can be observed in the NHHP spectrum (Figure 2b), which positions the side-chain to form a salt bridge to the β-phosphate and/or to the AlF_4^-. And indeed, a sidechain correlation peak involving ^{15}N is observed for 209K in both the hNH and NC spectrum (Figure 2c,e); observation of such cross signals is often related to involvement of the $N^{\zeta}H_3^+$ group in salt bridge formation[52]. Interestingly, the 209K H^N chemical shift represents the most deshielded ^{1}H resonance (11.0 ppm) for the DnaB:ADP:AlF_4^-:DNA complex. Also, an (ambiguous) signal is observed at the 209K H^N shift in the NHHP spectrum. 209K H^N is thus with high

confidence involved in a strong hydrogen bond which is established only on nucleotide-binding, since the 209K H^N resonance is not observed in the apo form. Such conclusion can be drawn from the hNH spectra shown in Figure 4 which compare the DnaB:ADP:AlF_4^-:DNA state with the pre-hydrolytic DnaB:AMP-PCP:DNA and the apo state. This agrees with previous findings that 209K stiffened upon ADP:AlF_4^- binding and remained flexible in the apo form, interestingly also in the DnaB:AMP-PCP:DNA state where one would also expect that 209K binds to the nucleotide (see Table S2 and Figure 4 for the 2D hNH spectra)[44].

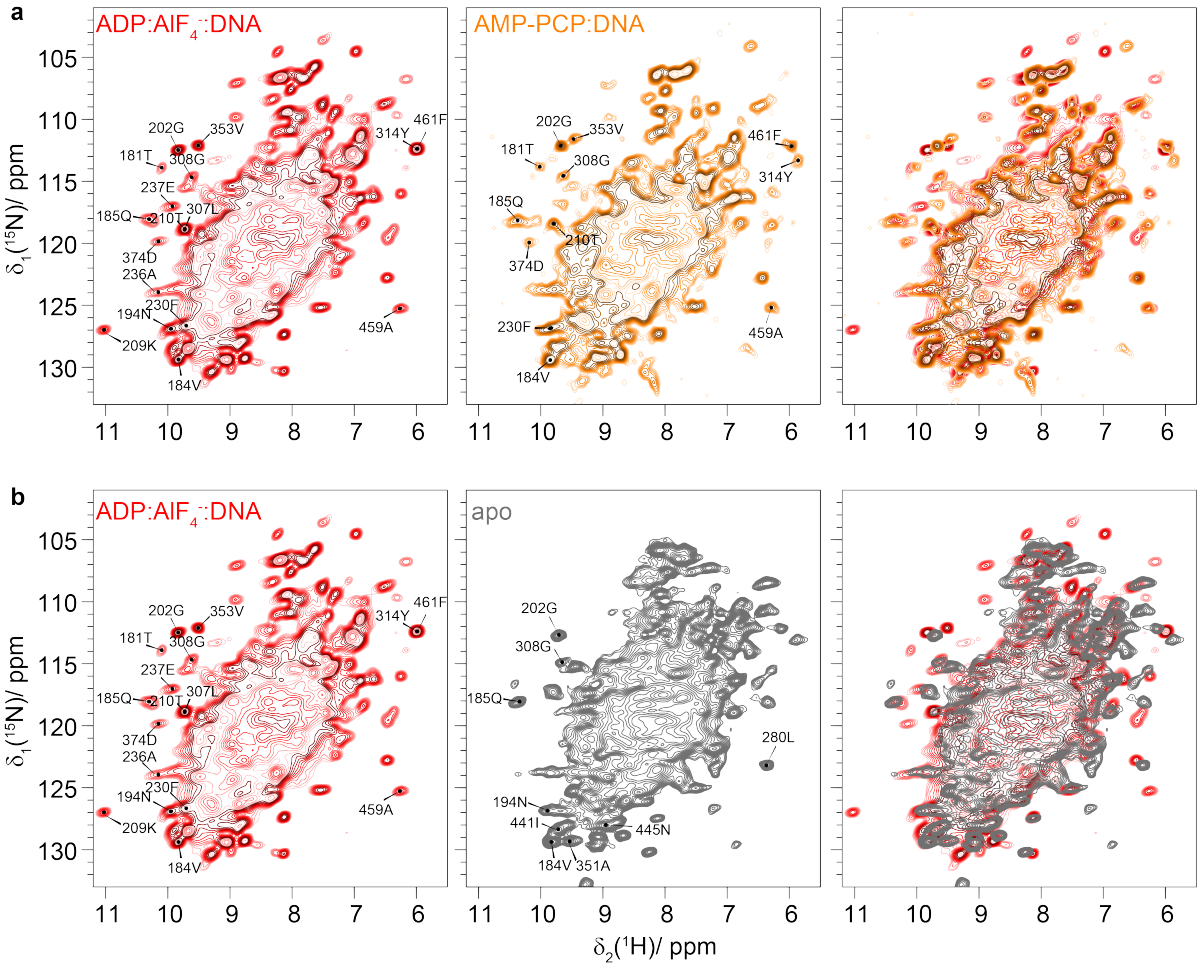

Figure 4: *Deshielded and shielded $^1H^N$ resonances differ between the DNA-bound and apo state.* **a** Comparison of 2D hNH spectra of DnaB:ADP:AlF_4^-:DNA (red) and DnaB:AMP-PCP:DNA (orange). Characteristic deshielded and shielded isolated peaks discussed in the main text are marked. **b** Comparison of 2D hNH spectra of DnaB:ADP:AlF_4^-:DNA (red) and apo DnaB (gray). Characteristic peaks are marked.

The NHHP spectrum indicates spatial proximity of further 209K-neighboring residues and the nucleotide among which 210T is most likely involved in hydrogen bonding (H^N shift of 9.7 ppm). 206S is also relatively deshielded (9.4 ppm) for DnaB:ADP:AlF_4^-:DNA. The equivalent residue to 206S has been identified in other NTPases, whose structures locate this

residue in the Walker A motif near the fluorine atom of the γ-phosphate mimic, identifying its key role in stabilizing the γ-phosphate during ATP hydrolysis[53].

Besides 209K, correlation signals for $N^{\eta1/\eta2}$ and N^{ε} side-chain resonances are observed in the NHHP/CHHP spectra for 446R, showing that it is in close spatial proximity to Pα of ADP (Figure 2b, S6). 446R is located in the R-finger which connects two adjacent monomers, and plays a central role in ATP binding and hydrolysis[1, 53-55]. While in the hNH spectrum (Figure 2a) the 446R resonances cannot be unambiguously assigned, a deshielded ^{1}H resonance (10.1 ppm) is particularly observed for $N^{\eta1/\eta2}$ at the corresponding ^{15}N shift, which could support assignments to this residue based on the expected hydrogen-bond formation with the ADP phosphate group.

The findings from the ^{31}P intermolecular correlation experiments and ^{1}H chemical shifts are summarized in Figure 5a, and are compared to the interactions available from the *Bst*DnaB:GDP:AlF_4^-:DNA crystal structure (Figure 5b). One can see that the contacts with the nucleotide as defined by NMR in DnaB are similar to those revealed by the X-ray structure for *Bst*DnaB, as for example the close spatial proximity of the equivalent to 209K lysine sidechain (216K) located in the Walker A motif to the nucleotide. Despite these similarities, NMR also reveals small differences in the binding mode, as for example the spatial proximity of the R-finger in DnaB:ADP:AlF_4^-:DNA (446R) exclusively to Pα as deduced from the NHHP and CHHP spectra (Figure 2b and Figure S6), which distinguishes it from *Bst*DnaB:GDP:AlF_4^-:DNA, where 420R is close to both GDP phosphate groups (Figure 5b)[7]. Note that there is an important difference between the *Bst*DnaB structure and our NMR data for *Hp*DnaB regarding the occupancy of ATP-binding sites. While for *Bst*DnaB only five out of six nucleotide binding domains are occupied, full occupancy was derived from the NMR data for *Hp*DnaB[44] still indicating structural differences between these proteins.

The DNA chemical-shift region of the NHHP spectrum in Figure 2b reveals two ^{31}P chemical shifts for two ^{31}P DNA phosphate resonances. The binding of two DNA nucleotides per DnaB monomer is a common feature of SF4 helicases[7, 44] and reflected in solid-state NMR by two ^{31}P resonances with different ^{31}P chemical-shift values (see Figure 6 for a 2D 150 ms ^{31}P-^{31}P DARR spectrum). Strong cross-peaks between the two ADP resonances indicate the close spatial proximity of the two ADP phosphate groups, while for the two DNA resonances such cross-peaks are less intense. The presence of the cross-peaks however still indicates that the two ^{31}P DNA resonances can be assigned to two structurally distinct but neighbored phosphate groups of DNA.

10.1002/cbic.201900439

Only one shows a correlation between the ^{31}P DNA resonance at highest ppm-values and the lysine sidechain of 373K (see Figure S7 for the assignment of this residue). The N^{ξ}-H^{ξ} side-chain resonance of this residue is also observed in the hNH spectrum (7.6 ppm, Figure 2c) supporting its involvement in a salt bridge with the DNA phosphate. For apo DnaB, no lysine sidechain correlations are detected, in line with our previous findings[44]. Concomitant to this, the neighboring residue, 374D shows a particularly deshielded resonance of 10.1 ppm, indicating that it is as well involved in a hydrogen bond, possibly with the DNA (see Figures 4 and 5 and Table S2).

10.1002/cbic.201900439

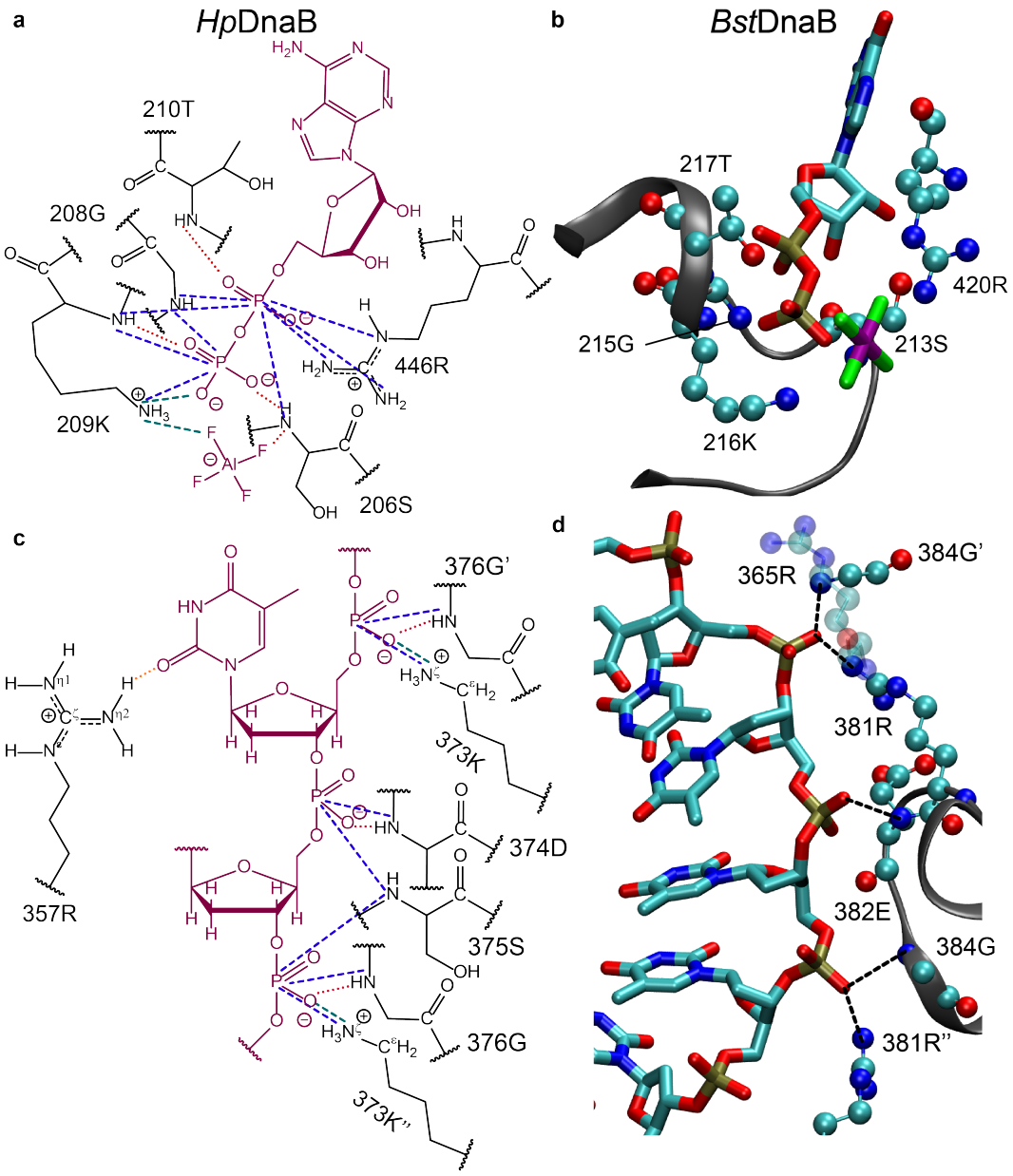

Figure 5: **Protein-nucleotide interactions in DnaB derived from solid-state NMR. a** Schematic drawing of protein-ADP:AlF_4^- (highlighted in magenta) contacts deduced from the NMR data (the broken lines represent spatial correlations observed in the NMR spectra with the corresponding color code used for the spectra in Figure 2 and the dotted lines represent hydrogen bonds derived from chemical shifts). **b** Protein-GDP:AlF_4^- contacts in *Bst*DnaB:DNA as determined from the crystal structure (PDB 4ESV[7]). **c** Schematic drawing of protein-DNA contacts similar to **a**. ´ and ´´ indicate residues from the adjacent chains. **d** Protein-DNA contacts in *Bst*DnaB:DNA as determined from the crystal structure (PDB 4ESV[7]).

Further interactions can be identified in the arginine side-chain region of the hNH spectrum in Figure 2d. The isolated 357R $^{15}N\eta2$ chemical-shift (Figure 2f and Figure S8) can be clearly identified. Two correlation peaks to ^{1}H are detected at this frequency, one around 10.2 ppm, and the other around 7.6 ppm (Figure S9). While the latter is a typical amide proton chemical-shift value, the first is deshielded, indicating hydrogen-bonding interactions, but no

correlations to the DNA phosphates are observed in NHHP (Figure 2b) and only very weak ones are seen in the CHHP spectra, in contrast to 446R of the R-finger (Figure S6). Arginine residues can show three different sidechain-DNA binding modes[4, 6]: either to the DNA phosphate group, to the base edges or to the ribose, via hydrogen bonding or electrostatic interactions or to the DNA base plane via electrostatic cation-π interactions[56-58]. The absence of NHHP correlations, combined with the deshielded proton shift, positions 357R in coordination with the DNA base edge. As only one H^N is deshielded, only one $N^{\eta}H_2$ moiety is involved in a hydrogen bond to one of the thymidine oxygens (see Figure 5c for a schematic drawing). The relatively broad resonances (predominantly in the ^1H dimension) might be a consequence of structural disorder, *e.g.* a small structural inequivalence of the DnaB monomers in the oligomeric protein-DNA complex, leading to a chemical-shift distribution. These observations show that NMR allows us to distinguish between hydrogen bonds to the DNA phosphate groups or to the DNA base edge. Arginine sidechain-thymidine DNA base edge interactions are rather rarely observed and much less frequent than for example arginine-guanidine pairs[4, 6].

Figure 5c schematically summarizes the obtained information on the DNA-binding mode of DnaB, and compares it to the DNA-binding modes from equivalent residues in the *Bst*DnaB:GDP:AlF_4^-:DNA structure[7]. 373K contacts the DNA phosphate backbone via a salt bridge, with nearby residues 374D-376G among which 374D and 376G are potentially also involved in binding based on their deshielded H^N resonances. 357R contacts possibly the DNA base edge via hydrogen bonding. Figure 5d shows that equivalent contacts can be seen in the crystal structure of *Bst*DnaB:GDP:AlF_4^-:DNA[7]), where the sidechain of 381R (corresponds to 373K in *Hp*DnaB) is in spatial proximity to the phosphate group of DNA, while the amide nitrogen atoms of 382E and 384G (374D and 376G, respectively, in *Hp*DnaB) contact the phosphate group of DNA possibly via hydrogen bonds. However, the analogue of 357R in *Bst*DnaB (365R) is close to the DNA phosphate groups in the crystal structure indicating still differences in DNA coordination.

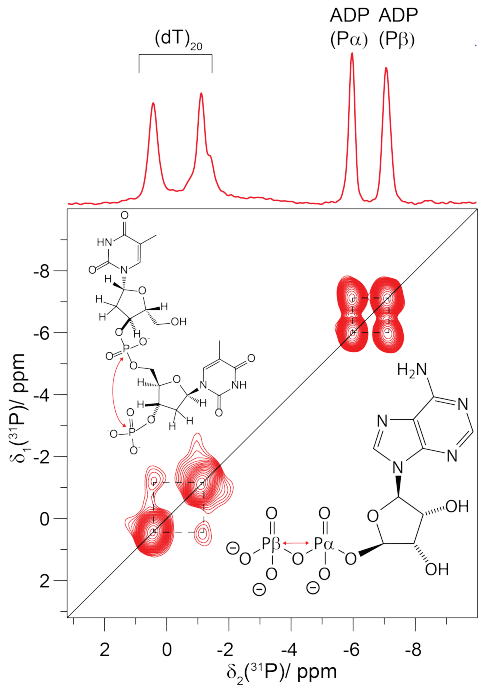

Figure 6: *Two DNA nucleotides bind per DnaB monomer and are in spatial proximity.* ^{31}P-^{31}P 150 ms DARR spectrum of DnaB:ADP:AlF_4:DNA showing that the two bound DNA nucleotides are in close spatial proximity. On top of the 2D spectrum, a ^{31}P CP spectrum is shown (taken from reference [44]).

In conclusion, we illustrated that a large part of the ^{1}H resonances in a motor protein assembly can be assigned by exploiting the well-dispersed H^N and H^A frequencies in a combined 3D assignment approach using four different spectra. We showed that NHHP spectra can be recorded with sufficient signal/noise, even if acquisition times remain long and demonstrated how information from both can be combined to identify and conclude on nucleotide binding modes, for both ATP and DNA. Our findings compare well with data on a related protein whose crystal structure is available, and validates the presented approach. The procedure described here shall thus allow to detect noncovalent interactions in molecular recognition processes involving nucleotides also in further non-crystalline protein assemblies, be it in the context of nucleic acid synthesis, extension, repair, or packaging, as typically occurring by capsids in viruses or with histones in chromosomes. Even the investigation of changes in protein-DNA contacts during functional cycles, e.g. in DNA replication, becomes accessible.

Acknowledgements

This work was supported by the Swiss National Science Foundation (Grant 200020_159707 and 200020_178792), the French ANR (ANR-14-CE09-0024B), the LABEX ECOFECT (ANR-11-LABX-0048) within the Université de Lyon program Investissements d'Avenir

(ANR-11-IDEX-0007), the ETH Career SEED-69 16-1 and the ETH Research Grant ETH-43 17-2. This project has received funding from the European Research Council (ERC) under the European Union's Horizon 2020 research and innovation programme (grant agreement n° 741863, FASTER). We thank Dr. Armen Mulkidjanian (University of Osnabrück, Germany) for helpful discussions.

References

[1] M. Spies, *DNA Helicases and DNA Motor Proteins*, Springer New York, **2012**.
[2] M. K. Levin, S. S. Patel, in *Molecular Motors*, Wiley-VCH Verlag GmbH & Co. KGaA, **2004**, pp. 179-203.
[3] P. A. Kollman, *Acc. Chem. Res.* **1977**, *10*, 365-371.
[4] D. Lejeune, N. Delsaux, B. Charloteaux, A. Thomas, R. Brasseur, *Proteins: Structure, Function, and Bioinformatics* **2005**, *61*, 258-271.
[5] S. Grimme, *Angew. Chem. Int. Ed.* **2008**, *47*, 3430-3434.
[6] N. M. Luscombe, R. A. Laskowski, J. M. Thornton, *Nucleic Acids Res.* **2001**, *29*, 2860-2874.
[7] O. Itsathitphaisarn, Richard A. Wing, William K. Eliason, J. Wang, Thomas A. Steitz, *Cell* **2012**, *151*, 267-277.
[8] C. Gardiennet, A. K. Schütz, A. Hunkeler, B. Kunert, L. Terradot, A. Böckmann, B. H. Meier, *Angew. Chem. Int. Ed.* **2012**, *51*, 7855-7858.
[9] S. Jehle, M. Falb, J. P. Kirkpatrick, H. Oschkinat, B.-J. van Rossum, G. Althoff, T. Carlomagno, *J. Am. Chem. Soc.* **2010**, *132*, 3842-3846.
[10] S. Asami, M. Rakwalska-Bange, T. Carlomagno, B. Reif, *Angew. Chem. Int. Ed.* **2013**, *52*, 2345-2349.
[11] W. Huang, G. Varani, G. P. Drobny, *J. Biomol. NMR* **2011**, *51*, 347.
[12] W. Huang, G. Varani, G. P. Drobny, *J. Am. Chem. Soc.* **2010**, *132*, 17643-17645.
[13] O. Morag, G. Abramov, A. Goldbourt, *J. Am. Chem. Soc.* **2014**, *136*, 2292-2301.
[14] L. B. Andreas, K. Jaudzems, J. Stanek, D. Lalli, A. Bertarello, T. Le Marchand, D. Cala-De Paepe, S. Kotelovica, I. Akopjana, B. Knott, S. Wegner, F. Engelke, A. Lesage, L. Emsley, K. Tars, T. Herrmann, G. Pintacuda, *Proc. Natl. Acad. Sci.* **2016**, *113*, 9187-9192.
[15] V. Agarwal, S. Penzel, K. Szekely, R. Cadalbert, E. Testori, A. Oss, J. Past, A. Samoson, M. Ernst, A. Böckmann, B. H. Meier, *Angew. Chem. Int. Ed.* **2014**, *53*, 12253-12256.
[16] D. Stöppler, A. Macpherson, S. Smith-Penzel, N. Basse, F. Lecomte, H. Deboves, R. D. Taylor, T. Norman, J. Porter, L. C. Waters, M. Westwood, B. Cossins, K. Cain, J. White, R. Griffin, C. Prosser, S. Kelm, A. H. Sullivan, D. Fox, III, M. D. Carr, A. Henry, R. Taylor, B. H. Meier, H. Oschkinat, A. D. Lawson, *PLOS Biology* **2018**, *16*, e2006192.
[17] J. Medeiros-Silva, S. Jekhmane, A. L. Paioni, K. Gawarecka, M. Baldus, E. Swiezewska, E. Breukink, M. Weingarth, *Nat. Commun.* **2018**, *9*, 3963.
[18] S. K. Vasa, H. Singh, K. Grohe, R. Linser, *Angew. Chem. Int. Ed. Engl.* **2019**, *58*, 5758-5762.
[19] J. Stanek, L. B. Andreas, K. Jaudzems, D. Cala, D. Lalli, A. Bertarello, T. Schubeis, I. Akopjana, S. Kotelovica, K. Tars, A. Pica, S. Leone, D. Picone, Z.-Q. Xu, N. E. Dixon, D. Martinez, M. Berbon, N. El Mammeri, A. Noubhani, S. Saupe, B. Habenstein, A. Loquet, G. Pintacuda, *Angew. Chem. Int. Ed.* **2016**, *55*, 15504-15509.
[20] Y. Nishiyama, M. Malon, Y. Ishii, A. Ramamoorthy, *J. Magn. Reson.* **2014**, *244*, 1-5.
[21] J. Struppe, C. M. Quinn, M. Lu, M. Wang, G. Hou, X. Lu, J. Kraus, L. B. Andreas, J. Stanek, D. Lalli, A. Lesage, G. Pintacuda, W. Maas, A. M. Gronenborn, T. Polenova, *Solid State Nucl. Magn. Reson.* **2017**, *87*, 117-125.
[22] T. Schubeis, T. Le Marchand, L. B. Andreas, G. Pintacuda, *J. Magn. Reson.* **2018**, *287*, 140-152.
[23] S. K. Vasa, P. Rovó, R. Linser, *Acc. Chem. Res.* **2018**, *51*, 1386-1395.
[24] G. A. Jeffrey, Y. Yeon, *Acta Crystallographica Section B* **1986**, *42*, 410-413.
[25] B. Berglund, R. W. Vaughan, *J. Chem. Phys.* **1980**, *73*, 2037-2043.
[26] M. Barfield, *J. Am. Chem. Soc.* **2002**, *124*, 4158-4168.

[27] L. L. Parker, A. R. Houk, J. H. Jensen, *J. Am. Chem. Soc.* **2006**, *128*, 9863-9872.
[28] R. K. Harris, R. E. Wasylishen, M. J. Duer, *NMR Crystallography*, Wiley, **2012**.
[29] G. Wagner, A. Pardi, K. Wuethrich, *J. Am. Chem. Soc.* **1983**, *105*, 5948-5949.
[30] T. Asakura, K. Taoka, M. Demura, M. P. Williamson, *J. Biomol. NMR* **1995**, *6*, 227-236.
[31] N. E. Zhou, B. Y. Zhu, B. D. Sykes, R. S. Hodges, *J. Am. Chem. Soc.* **1992**, *114*, 4320-4326.
[32] F. Cordier, S. Grzesiek, *J. Am. Chem. Soc.* **1999**, *121*, 1601-1602.
[33] S. J. Perkins, K. Wüthrich, *Biochimica et Biophysica Acta (BBA) - Protein Structure* **1979**, *576*, 409-423.
[34] D. Sitkoff, D. A. Case, *J. Am. Chem. Soc.* **1997**, *119*, 12262-12273.
[35] D. A. Case, *J. Biomol. NMR* **1995**, *6*, 341-346.
[36] D. S. Wishart, B. D. Sykes, F. M. Richards, *J. Mol. Biol.* **1991**, *222*, 311-333.
[37] A. Bazin, M. V. Cherrier, I. Gutsche, J. Timmins, L. Terradot, *Nucleic Acids Res.* **2015**, *43*, 8564-8576.
[38] J. E. Walker, M. Saraste, M. J. Runswick, N. J. Gay, *EMBO J.* **1982**, *1*, 945-951.
[39] J. L. Kellie, K. A. Wilson, S. D. Wetmore, *Nucleic Acids Res.* **2014**, *42*, 6726-6741.
[40] H. W. Mackenzie, D. F. Hansen, *J. Biomol. NMR* **2017**, *69*, 123-132.
[41] A. Esadze, C. Chen, L. Zandarashvili, S. Roy, B. M. Pettitt, J. Iwahara, *Nucleic Acids Res.* **2016**, *44*, 6961-6970.
[42] B. Raman, C. Guarnaccia, K. Nadassy, S. Zakhariev, A. Pintar, F. Zanuttin, D. Frigyes, C. Acatrinei, A. Vindigni, G. Pongor, S. Pongor, *Nucleic Acids Res.* **2001**, *29*, 3377-3384.
[43] D. Frigyes, F. Alber, S. Pongor, P. Carloni, *Journal of Molecular Structure: THEOCHEM* **2001**, *574*, 39-45.
[44] T. Wiegand, R. Cadalbert, D. Lacabanne, J. Timmins, L. Terradot, A. Bockmann, B. H. Meier, *Nat. Commun.* **2019**, *10*, 31.
[45] T. Wiegand, R. Cadalbert, C. von Schroetter, F. H.-T. Allain, B. H. Meier, *J. Biomol. NMR* **2018**, *71*, 237-245.
[46] A. Schuetz, C. Wasmer, B. Habenstein, R. Verel, J. Greenwald, R. Riek, A. Böckmann, B. H. Meier, *ChemBioChem* **2010**, *11*, 1543-1551.
[47] Y. Wang, O. Jardetzky, *Protein Science : A Publication of the Protein Society* **2002**, *11*, 852-861.
[48] S. Penzel, A. Oss, M.-L. Org, A. Samoson, A. Böckmann, M. Ernst, B. H. Meier, *J. Biomol. NMR* **2019**.
[49] D. Cala-De Paepe, J. Stanek, K. Jaudzems, K. Tars, L. B. Andreas, G. Pintacuda, *Solid State Nucl. Magn. Reson.* **2017**, *87*, 126-136.
[50] A. Lange, S. Luca, M. Baldus, *J. Am. Chem. Soc.* **2002**, *124*, 9704-9705.
[51] M. Stelter, I. Gutsche, U. Kapp, A. Bazin, G. Bajic, G. Goret, M. Jamin, J. Timmins, L. Terradot, *Structure* **2012**, *20*, 554.
[52] K. M. Sepuru, J. Iwahara, K. Rajarathnam, *Analyst* **2018**, *143*, 635-638.
[53] D. N. Shalaeva, D. A. Cherepanov, M. Y. Galperin, A. V. Golovin, A. Y. Mulkidjanian, *eLife* **2018**, *7*, e37373.
[54] Y. Jin, R. W. Molt, G. M. Blackburn, *Top. Curr. Chem.* **2017**, *375*, 36.
[55] T. Ogura, S. W. Whiteheart, A. J. Wilkinson, *J. Struct. Biol.* **2004**, *146*, 106-112.
[56] J. P. Gallivan, D. A. Dougherty, *Proc. Natl. Acad. Sci.* **1999**, *96*, 9459-9464.
[57] S. Burley, G. Petsko, *Science* **1985**, *229*, 23-28.
[58] J. C. Ma, D. A. Dougherty, *Chem. Rev.* **1997**, *97*, 1303-1324.